J Solid State Electrochem (1999) 3: 464–469 © Springer-Verlag 1999

SHORT COMMUNICATION

K.M. Shaju · V. Ganesh Kumar
N. Munichandraiah · A.K. Shukla

Performance and scaling of a 1.2 V/1.5 Ah nickel/metal hydride cell to a 6 V/1.5 Ah battery

Received: 17 November 1998 / Accepted: 5 February 1999

Abstract A 1.2 V/1.5 Ah positive-limited nickel/metal hydride cell has been studied to determine its charge-discharge characteristics at different rates in conjunction with its AC impedance data. The faradaic efficiency of the cell is found to be maximum at ~70% charge input. The cell has been scaled to a 6 V/1.5 Ah battery. The cycle-life data on the battery suggest that it can sustain a prolonged charge-discharge schedule with little deterioration in its performance.

Key words Nickel/metal hydride battery · AB_2 alloy · AC impedance

Introduction

There is a rapidly increasing need for portable stored-energy derived from electricity, particularly in a rechargeable form. Electrochemical energy stored in secondary batteries has long been used for this purpose. However, for the new generation of electronic applications like the 3Cs appliances, viz. cellular phones, camcorders, and laptop computers, the stored energy density of the existing battery systems is inadequate and is limiting the introduction of more sophisticated units. Besides, there is a world-wide interest in developing storage batteries for viable electric vehicles. Although presently available lead-acid secondary batteries are capable of being scaled for this purpose at a reasonable cost, these are unacceptable owing to their limited energy density. Among the newer secondary batteries capable of giving a several-fold improvement in energy density over the lead-acid system, the nickel/metal hydride (Ni/MH) technology is well regarded as one of the best prospects [1–4].

A key factor for the development of the Ni/MH battery is the selection of an appropriate hydrogen storage alloy to function as the negative electrode [4–7]. Among the various alloys that have been employed as negative electrode materials in Ni/MH cells, the AB_2 and AB_5 series of alloys are the most promising. Each of these alloys has its own specific advantages and disadvantages to function as an efficient negative electrode material for the secondary Ni/MH battery. A literature survey on the materials aspects of metal hydrides as battery electrodes suggests that, although initially AB_5 alloys were mainly used for battery application, the present interest is more in AB_2 alloys [8]. Among the latter class of alloys, the zirconium-based laves phases have been documented to be the most attractive metal hydride electrode materials [9, 10]. Although these materials have been successfully employed for developing Ni/MH storage batteries, the data on the performance and scaling problems of the component cells comprising these batteries are rather scanty in the literature.

In this communication, we therefore report the performance and scaling of a positive-limited 1.2 V/1.5 Ah Ni/MH cell to a 6 V/1.5 Ah battery. The data suggest that the cells can be charged up to about 70% of their rated capacity with nearly 100% faradaic efficiency[1]. The cycle-life data on the cell and the battery suggest that both can sustain prolonged charge-discharge schedules with little deterioration in their capacity.

K.M. Shaju · V. Ganesh Kumar · A.K. Shukla (✉)
Solid State and Structural Chemistry Unit,
Indian Institute of Science, Bangalore – 560012, India
e-mail: shukla@sscu.iisc.ernet.in

N. Munichandraiah
Department of Inorganic and Physical Chemistry,
Indian Institute of Science, Bangalore – 560012, India

[1] Faradaic efficiency is the ratio of the output of the cell on discharge to the input required to store it to its initial state-of-charge, (SOC) which is the ratio of the available capacity to the maximum attainable capacity

Experimental

Alloy preparation

A zirconium-based laves phase alloy of nominal composition $Zr_{0.5}Ti_{0.5}V_{0.6}Cr_{0.2}Ni_{1.2}$ has been employed for the present study. The alloy, weighing about 600 g, was obtained as an ingot by repeated arc melting its spongy constituent elements under an argon atmosphere at $\sim 10^{-3}$ Pa in a water-cooled copper crucible. The formation of the alloy was confirmed from its powder X-ray diffraction pattern. The composition of the alloy as determined from energy dispersive analysis by X-rays was $Zr_{0.49}Ti_{0.46}V_{0.65}Cr_{0.21}Ni_{1.19}$. The alloy was pulverized mechanically and was passed through graded sieves to obtain alloy particles in the range 49–73 μm (200–300 mesh, average particles size: 60 μm).

Electrode preparation

Roll-compacted metal hydride electrodes were prepared from the alloy powder. The dough obtained by mixing alloy (85 wt%), graphite (10 wt%) and polytetrafluoro-ethylene (GP2 Fluon) suspension (5 wt%) was rolled into thin sheets and folded around a degreased nickel mesh (dimensions: 56 mm × 50 mm × 0.1 mm) to obtain an electrode of ~1 mm thickness. The electrode contained ~100 mg of the active material per cm^2. The electrodes were compacted at an optimum pressure of 3000 kg cm^{-2} for 15 min followed by heat treating in a gas stream comprising 10% hydrogen and 90% argon at 623 K for 30 min. Commercial grade nickel-positive electrodes (dimensions: 1 mm × 56 mm × 50 mm) were employed for the cell and battery assemblies.

Cell and battery assemblies

Positive-limited Ni/MH secondary cells were assembled by alternately stacking three metal-hydride negative electrodes (average capacity: 0.8 Ah) and two commercial-grade nickel positives (average capacity: 0.8 Ah). The positive and negative electrodes were welded to their respective lugs and then placed in a plexiglass container (dimensions: 80 mm × 53 mm × 17 mm). The cell was then filled with 6 M KOH electrolyte so as to soak the electrodes completely. The container was then sealed with a provision to collect the evolved gas during the cell charging. The cell also had the provision to insert a micro-tipped Hg/HgO, OH^- (6 M KOH) reference electrode (MMO) to monitor the individual electrode performance .

A positive-limited 6 V/1.5 Ah battery was assembled in a specially designed plexiglass container with five compartments (Fig. 1). Each cell in the battery comprised alternately stacked three metal hydride negatives and two nickel positive electrodes akin to the configuration adopted for the assembly of 1.2 V/1.5 Ah cell. The cells were then connected in series to form a 6 V/1.5 Ah battery. All the measurements were performed at 30 ± 2 °C.

Electrochemical measurements

Both the cell and the battery were subjected to five charge-discharge formation cycles at a C/10 rate. Subsequently, a charge-discharge schedule with a C/5 rate was adopted. The performance of the individual electrodes in the fully formed cell was also monitored.

AC impedance measurements

The electrochemical impedance measurements of the cell at its different SOC values were obtained by using an Electrochemical Impedance Analyzer (EG&G PARC Model 6310) coupled to an IBM-PC and driven by EG&G Model 398 Software, in the frequency range 5 mHz–100 kHz with a signal amplitude of 5 mV. The SOC value for the cell at cut-off-voltage of 1 V was taken as zero during the present study. For impedance measurements, the cell was charged (or discharged) to a particular SOC value under constant-current mode at the C/5 rate and was allowed to stand for about two hours, under open-circuit conditions, prior to each measurement. The cell resistance values were obtained by analysing the impedance data using a non-linear least-squares (NLLS) fitting program [11].

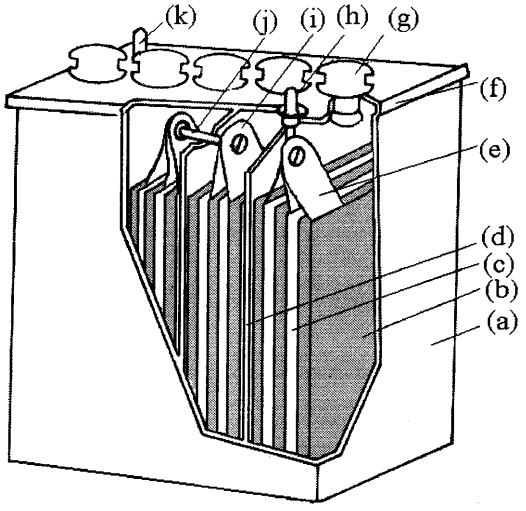

Fig. 1 Schematic diagram of the 6 V/1.5 Ah nickel/metal hydride battery. *a* Cell container, *b* negative electrode wrapped with separator cloth, *c* positive electrode, *d* cell separating wall, *e* negative lugs, *f* battery lid, *g* vent, *h* negative terminal, *i* positive lugs, *j* interconnection, and *k* positive terminal

Results and discussion

Typical charge and discharge data for the 1.2 V/1.5 Ah Ni/MH cell along with the charge-discharge data for individual nickel positive and metal hydride negative electrodes at the C/5 rate are shown in Fig. 2a and b, respectively. The cell was discharged up to a cut-off voltage of 1 V and its SOC value at this voltage was taken as zero; the corresponding potentials of the nickel positive and metal hydride negative electrodes with respect to MMO are 0.16 V and −0.84 V, respectively. From the individual electrode data, it is seen (Fig. 2) that the cell capacity was limited by its positive electrodes. The cell delivered an average capacity of 1.5 Ah at the C/5 rate of discharge (corresponding current: 0.3 A).

In a positive-limited Ni/MH cell, overcharge would cause oxygen evolution at the positive electrodes in accordance with the reaction [1, 12]: $4OH^- \rightarrow 2H_2O + O_2 + 4e^-$. Accordingly, at the later stages of cell and battery charging, the conversion of $Ni(OH)_2$ to NiOOH is accompanied by an oxygen evolution reaction (OER) at the nickel-positive electrodes. In this study, the cells were designed so that no hydrogen gas was generated at the metal hydride electrodes. The OER at the

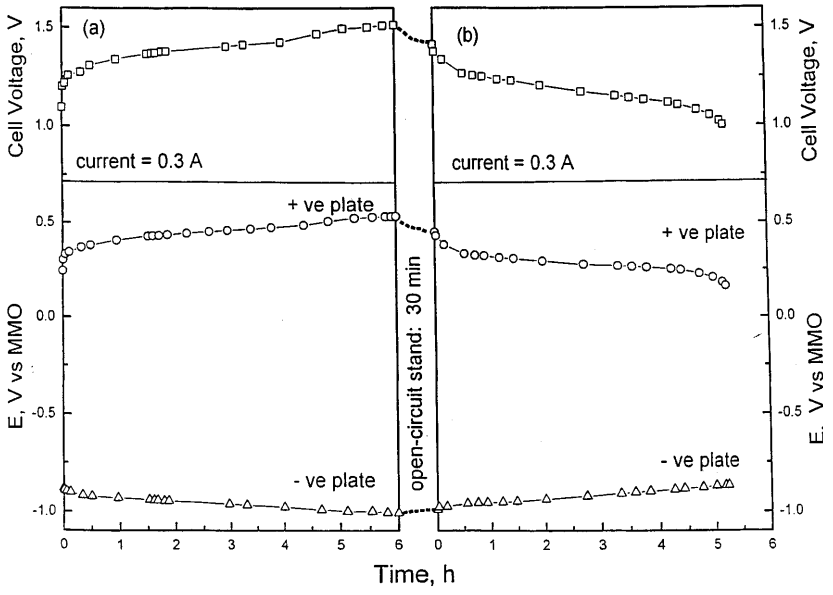

Fig. 2 **a** Charge and **b** discharge characteristics for the 1.2 V/1.5 Ah nickel/metal hydride cell and individual electrodes

nickel-positive electrodes would affect the faradaic efficiency of both the cell and the battery. The data on the volume of oxygen gas evolved at the nickel positives during the cell charging at various rates are shown in Fig. 3a. It is clear that there was little evolution of oxygen at the electrodes up to a charge input of ca. 70% (Fig. 3b).

The faradaic efficiency and capacity data for the cell obtained at the C/5 and C/2 rates are shown in Fig. 4. The faradaic efficiency was ~100% up to ~70% of charge input and decreased thereafter owing to parasitic reactions. Similar data have been reported recently for commercial Ni/MH cells [13]. The faradaic efficiency of the cell (Fig. 4) was found to decrease slightly as the charging rate increased from C/5 to C/2. This is because at the C/2 rate of cell charging, the rate of the OER was also relatively higher and hence more consumption of charge for the process.

The OER can bring about a change in the internal resistance of the cell due to: (1) the resistive shield on the active electrodes formed by evolved oxygen, and (2) the dilution of the electrolyte. A part of the evolved oxygen may get trapped inside the electrode pores and increase the internal resistance of the cell. Besides, the water produced during the OER will dilute the electrolyte, leading to an increase in the internal resistance of the cell. This behaviour is reflected in the impedance data of the cell. The impedance data measured at several SOC

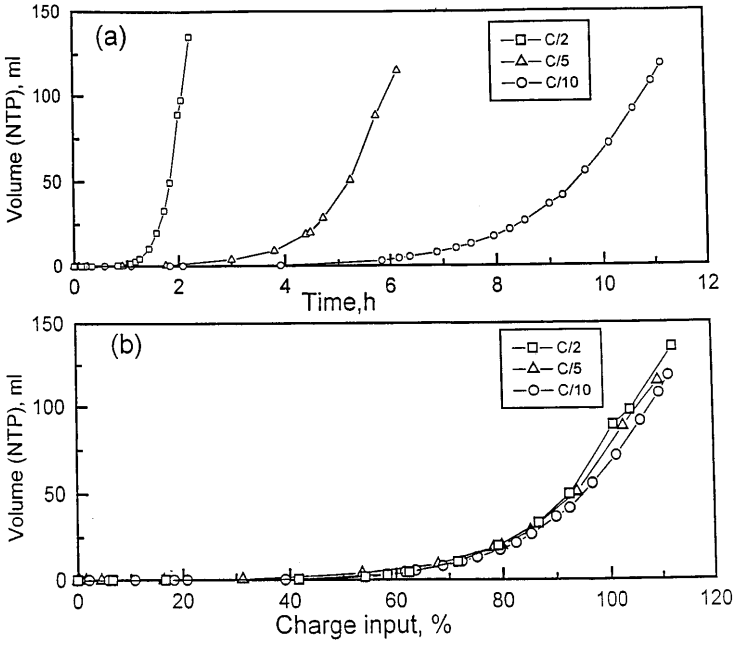

Fig. 3 Volume of oxygen at NTP collected during charging of 1.2 V/1.5 Ah nickel/metal hydride cell at C/2, C/5 and C/10 rates against charging time (**a**) and against charge input (**b**)

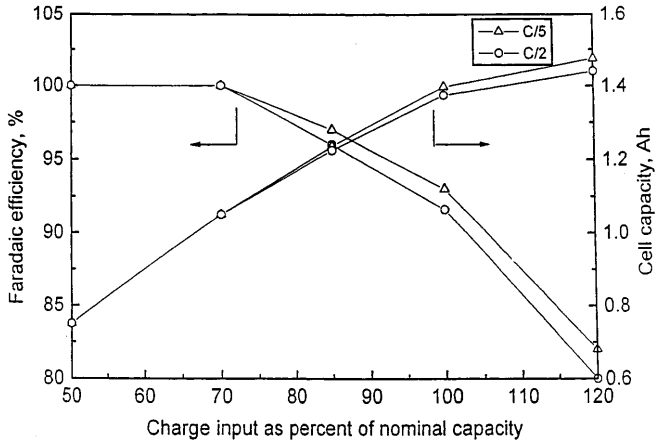

Fig. 4 Capacity and faradaic efficiency data at C/2 and C/5 rates for the 1.2 V/1.5 Ah nickel/metal hydride cell for different charge inputs

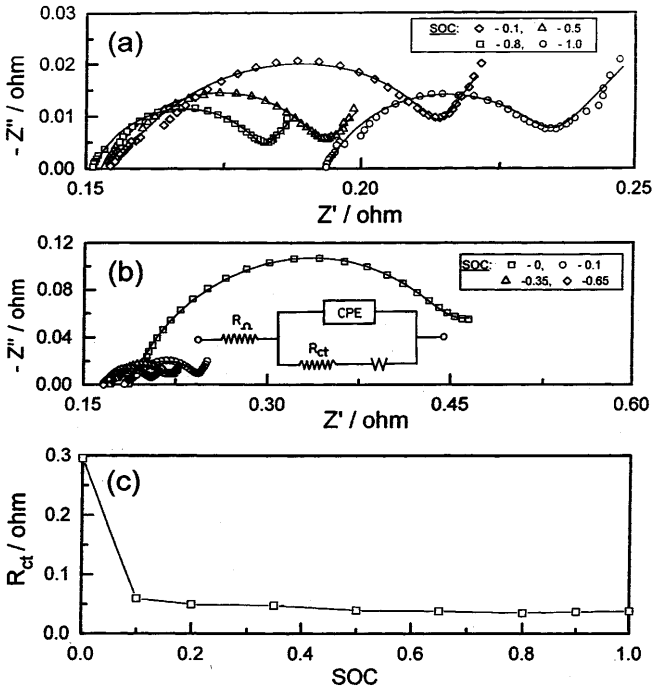

Fig. 5 Complex-impedance plots for the 1.2 V/1.5 Ah nickel/metal hydride cell at different SOC values: **a** during charge, **b** during discharge and **c** the SOC dependence of charge-transfer resistance as obtained from the impedance plots recorded during discharge. The experimental data are shown by *symbols* and the theoretical curves by *solid lines* in **a** and **b**. The equivalent circuit is shown in **b**

values of the cell are shown in Fig. 5a and b, each SOC value in Fig. 5a being reached by charging and in Fig. 5b by discharging the cell at the C/5 rate. Normally, the resistance value obtained from the high-frequency intercept of the semicircle represents the ohmic resistance (R_Ω) of the cell [14, 15], which comprises the resistances of the electrolyte, electrodes, current collectors, tags, terminals, etc. The resistance value obtained from the diameter of the semicircle is generally attributed to the charge-transfer resistance (R_{ct}) at the electrodes of the cell [15–17]. Since the semicircle is due to a parallel arrangement of R_{ct} and double-layer capacitance (C_{dl}), the parameters were evaluated using the equivalent circuit shown in Fig. 5b and the NLLS fitting program. The replacement of C_{dl} by a constant-phase element produced a good fit. It is evident from Fig. 5a that the ohmic resistance of the cell at SOC ~1 is greater than that at SOC ≤ 0.8 by about 50 mohm, thus explaining the effect of the OER. The value of R_{ct} obtained at both the SOC values, however, remains the same. Prior to each impedance measurement, the cell was at open-circuit stand for ~2 h, during which the evolved oxygen has enough time to diffuse and recombine with the active material at the negative electrodes [1, 12], according to the reaction: $4MH + O_2 \rightarrow 4M + 2H_2O$. Besides, ox-

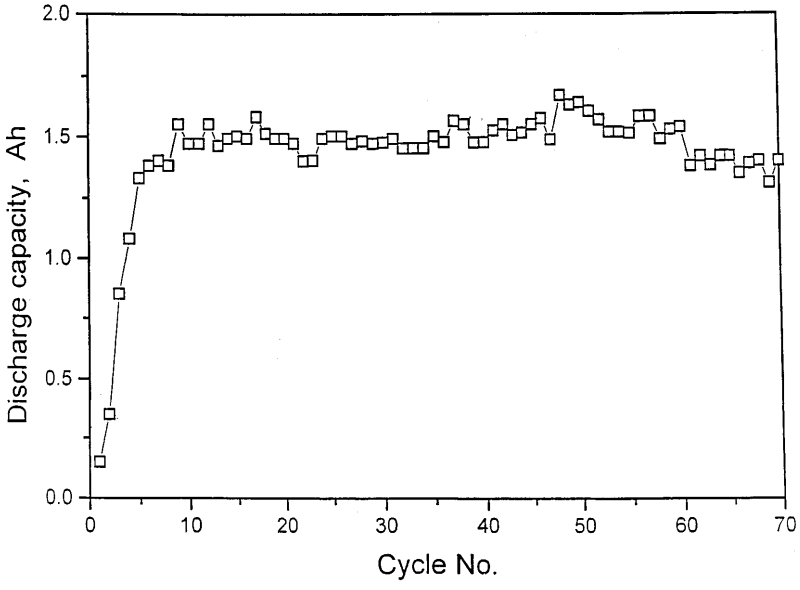

Fig. 6 Cycle-life data for the 1.2 V/1.5 Ah nickel/metal hydride cell

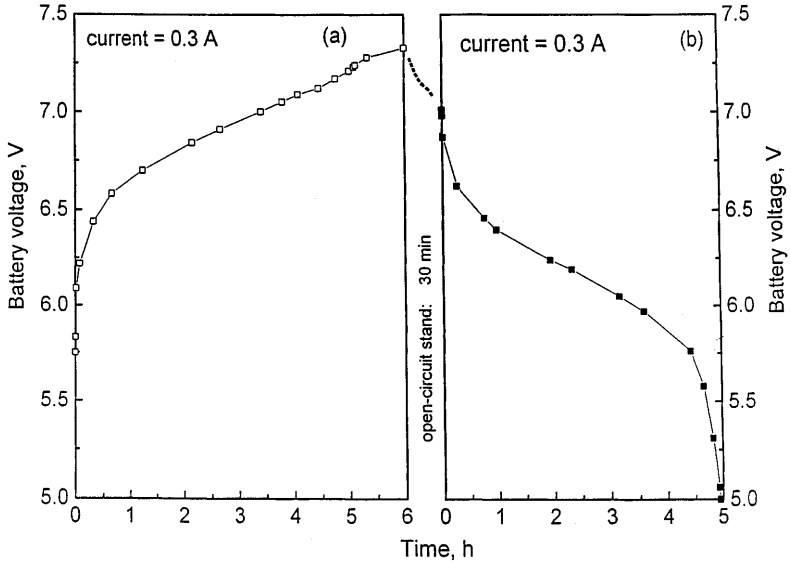

Fig. 7 **a** Charge and **b** discharge characteristics for the 6 V/1.5 Ah nickel/metal hydride battery

ygen can undergo reduction to hydroxyl ions following the reaction: $O_2 + 2H_2O + 4e^- \rightarrow 4OH^-$, during the initial stage of cell discharge. The latter process would add to the electrolyte conductivity. The impedance data obtained during the discharge of the cell (Fig. 5b) show little change in its ohmic resistance at SOC values between 0 and 1. The impedance plots at SOC ~1 of the cell during its charge and discharge are identical. It is noteworthy that no electrolyte dilution occurs during the cell discharge. The R_{ct} value of the cell as a function of its SOC is shown in Fig. 5c. The data show a sharp increase in R_{ct} values at SOC ~0.1, which is in agreement with the variation of R_{ct} reported for commercial Ni/MH cells [18, 19]. This increase in R_{ct} values has been attributed to the restricted electrode kinetics owing to the formation of an oxide film on the surface of the electrode active material [16, 20].

The cycle-life data for the 1.2 V/1.5 Ah Ni/MH cell are shown in Fig. 6. The cell took about 5 cycles for its formation and thereafter delivered a nearly stable capacity of ca. 1.5 Ah. The charge-discharge data for the 6 V/1.5 Ah battery at the C/5 rate are shown in Fig. 7. The battery delivered an average capacity of 1.5 Ah at the C/5 rate. The cycle-life data for the battery at the C/5 rate are shown in Fig. 8. Akin to the cell, the battery also took about 5 cycles for its formation and thereafter delivered a stable capacity of ~1.5 Ah.

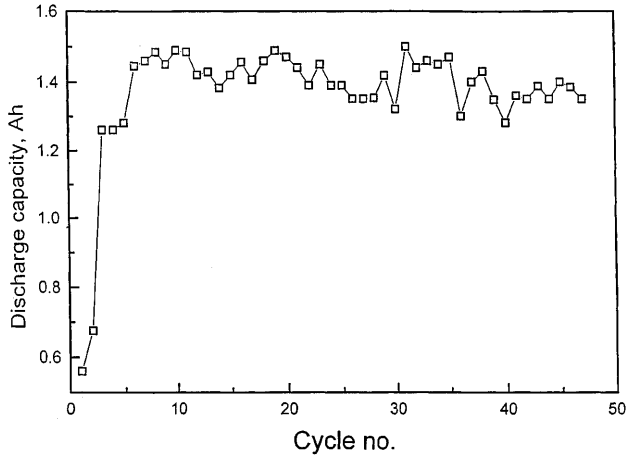

Fig. 8 Cycle-life data for the 6 V/1.5 Ah nickel/metal hydride battery

Conclusion

The charge-discharge studies on the 1.2 V/1.5 Ah Ni/MH cell studied here suggest that the cell can operate at nearly 100% faradaic efficiency up to the charge inputs of about 70%. The change in the internal impedance during its operation seems to be mainly due to its ohmic resistance owing to the OER. The cell can sustain a prolonged charge-discharge schedule with little deterioration and can be scaled up to a battery with similar performance.

Acknowledgements K.M.S is grateful to Council of Scientific and Industrial Research, New Delhi (India), for financial support. Our thanks are also due to DMRL-Hyderabad and M/S Renewable Energy Systems-Hyderabad for their help.

References

1. Linden D (1995) Sealed nickel-metal hydride batteries. In: Linden D (ed) Handbook of batteries. McGraw Hill, New York, pp 33.1–33.29
2. Ovshinsky SR, Fetcenko MA, Ross J (1993) Science 260: 176
3. Dhar SK, Ovshinsky SR, Gifford PR, Corrigan DA, Fetcenko MA, Venkatesan S (1997) J Power Sources 65: 1
4. Fetcenko MA, Venkatesan S, Ovshinsky SR (1992) Selection of metal-hydride alloys for electrochemical applications. In: Corrigan DA, Srinivasan S (eds) Proceedings of The Electrochemical Society, vol 92-5. The Electrochemical Society, Pennington, NJ, p 141

5. Petrov K, Rostami AA, Visintin A, Srinivasan S (1994) J Electrochem Soc 141: 1747
6. Anani A, Visintin A, Petrov K, Srinivasan S, Reilly JJ, Johnson JR, Schwarz RB, Desch PB (1994) J Power Sources 47: 261
7. Yu J-S, Liu B-H, Cho K, Lee J-Y (1998) J Alloys Compd 278: 283
8. Reference deleted
9. Ganesh Kumar V, Shaju KM, Munichandraiah N, Shukla AK (1998) J Power Sources 76: 106
10. Knosp B, Jordy C, Blanchard P, Berlureau T (1998) J Electrochem Soc 145: 1478
11. Boukamp BA (1989) Equivalent circuit, users manual. University of Twente, Netherlands
12. Ikoma M, Yuasa S, Yuasa K, Kaida S, Matsumoto I, Iwakura C (1998) J Alloys Compd 267: 252
13. Nagarajan GS, Van Zee JW (1998) J Power Sources 70: 173
14. Huet F (1998) J Power Sources 70: 59
15. Zhang L (1998) Electrochim Acta 43: 3333
16. Zhang W, Sridhar Kumar MP, Srinivasan S, Ploehn HJ (1995) J Electrochem Soc 142: 2935
17. Lee S-M, Kim D-M, Yu J-S, Jang K-J, Lee J-Y (1998) J Electrochem Soc 145: 1953
18. Bundy K, Karlsson M, Lindbergh G, Lundqvist A (1998) J Power Sources 72: 118
19. Ganesh Kumar V, Munichandraiah N, Shukla AK (1996) J Power Sources 63: 203
20. Hu W-K, Kim D-M, Jang K-J, Lee J-Y (1998) J Alloys Compd 269: 254